Experimental Investigations of the Stress Path Dependence of Weakly Cemented Sand

Ramesh Kannan Kandasami, Ph.D.[1]; Saurabh Singh, Ph.D.[2]; and Tejas Gorur Murthy, Ph.D.[3]

Abstract: Cohesion between grains in a geological system is perhaps the simplest and ideal representation of a range of material systems including soft rocks, structured soils, mudstones, cemented sands, powder compacts, and carbonate sands. This presence of inter granular cohesion is known to alter the ensemble mechanical response when subjected to varied boundary conditions. In this study, a hollow cylinder apparatus is used to investigate the mechanical behavior of weakly cemented sand ensembles by mapping the state boundary surfaces including the failure surface (locus of peak stress state) and the state of plastic flow (locus of final stress state). When these materials are sheared, the plastic deformation accumulates due to breakdown of cohesion between the grains, which introduces a lag in occurrence of peak stress ratio and maximum dilatancy, unlike a typical frictional granular material. This breakdown of cementation is affected by changes in the initial mean effective stress, initial reconstitution density, and intermediate principal stress ratio (stress path on the octahedral plane). The final state locus, emergent at large strains, was found to depend on the initial reconstitution density. Further, the parameters are extracted for calibration and prediction exercise using an elastic plastic constitutive model. In this and several other models, the effect of cementation is considered as an additional confinement to the ensemble. Such an approach predicts the stress state precisely but does not predict the volumetric response accurately, especially at large strains. **DOI: 10.1061/(ASCE)GT.1943-5606.0002475.**

Author keywords: Intermediate principal stress ratio; Initial reconstitution density; Additional confinement; Elastic-plastic surfaces.

Introduction

Engineering of infrastructure and offshore structures on and with geomaterials have utilized the continuum theory of plasticity to study, model, and predict their mechanical behavior. Traditionally, geoengineering has placed emphasis on design principles based on textbook soils (Carraro and Salgado 2004) wherein the inter grain interaction is predominantly due to friction. In the natural state, granular soils exist with weak cohesive bonds between the particles because of the presence of moisture, silicates, carbonates, and other organic matter (Clough et al. 1981; O'Rourke and Crespo 1988). Often, cohesion is also artificially introduced between particles, especially in soil improvement as a technique for enhancing strength and mitigating sand liquefaction. The presence of this interparticle cohesion imparts an inherent structure in the granular ensemble (Burland 1990).

Sampling of naturally structured sand is extremely challenging; hence, often weakly cemented geomaterials are artificially reconstituted in the laboratory (Clough et al. 1981; Coop and Atkinson 1993). Traditional geotechnical elemental tests have been used to study the mechanical behavior of cemented geomaterials in the laboratory. The dependence of stress history, initial density, structure-fabric, amount of cohesion, confining pressure, and type of cementing agent (Coop and Atkinson 1993; Abdulla and Kiousis 1997a; Airey 1993; Fernandez and Santamarina 2001; Huang and Airey 1998; Ismail et al. 2002; Lade and Overton 1989; Leroueil and Vaughan 1990; Rad and Clough 1982; Schnaid et al. 2001) have been reported through continuum level experiments. With an increase in cohesion between the grains, the elastic stiffness increases along with enhanced peak strength, which is mobilized at smaller strains. Further, the postpeak behavior shows a transition from ductile to brittle response with increasing density and decreasing mean effective stress (Lade and Overton 1989; Schnaid et al. 2001). Tests using the torsional shear and true triaxial apparatus have been used to explore the material response under general stress states, wherein the dimensionless parameter b and intermediate principal stress ratio (Bishop 1966) ($b = [\sigma_2' - \sigma_3']/[\sigma_1' - \sigma_3']$) has been used to map the three-dimensional (3D) stress state. Reddy and Saxena (1992, 1993) utilized a true triaxial apparatus to experimentally determine the failure locus for cemented sand.

In order to model the mechanical behavior of weakly cemented materials, several phenomenological elastic-plastic constitutive models have been formulated with strong experimental underpinning (Reddy and Saxena 1992; Gao and Zhao 2012; Gens and Nova 1993; Kim and Lade 1988; Lade and Kim 1988a, b; Vatsala et al. 2001). These models are able to predict the ensemble level behavior of weakly cemented materials to a reasonable extent. Despite the preponderance of studies on cemented geomaterials, especially utilizing traditional elemental tests, and consequent modeling using plasticity theory, a complete picture of the mechanical behavior of weakly cemented geomaterials has not emerged. Studies on the concomitant effect of mean effective stress, density/packing, and intermediate principal stress ratio on the mechanical response of weakly cemented geomaterials are few. In this study, the results

[1]Dept. of Civil Engineering, Indian Institute of Technology Madras, Chennai, India (corresponding author). ORCID: https://orcid.org/0000-0003-0803-3109. Email: rameshkk@iitm.ac.in

[2]Dept. of Civil Engineering, Indian Institute of Science, Bengaluru, India.

[3]Dept. of Civil Engineering, Indian Institute of Science, Bengaluru, India.

Note. This manuscript was submitted on June 6, 2019; approved on October 21, 2020No Epub Date. Discussion period open until 0, 0; separate discussions must be submitted for individual papers. This paper is part of the ***Journal of Geotechnical and Geoenvironmental Engineering***, © ASCE, ISSN 1090-0241.

of a laboratory program on weakly cemented sand specimens using a hollow cylinder apparatus are presented. Further, the effect of density, mean effective stress, and stress path on the octahedral plane in addition to obtaining a final state locus is examined. The stress dilatancy response of this weakly cemented sand as opposed to a purely frictional material has also been detailed.

Traditionally phenomenological plasticity models for such materials have used the interparticle cohesion as an additional confinement on a purely frictional material response. The efficacy of such a treatment of cohesion in an elastic-plastic single hardening constitutive model will be examined. The data set obtained from this experimental study will also be useful in benchmarking existing constitutive models or developing new ones for solving complex engineering boundary value problems more precisely and accurately.

Experimental

Hollow Cylinder Apparatus

Hollow cylinder torsion (HCT) apparatus is used in this study for conducting elemental tests on cemented sand. By controlling the axial load (F_v), torque (M), internal (p_i), and external (p_o) pressure on a hollow cylinder specimen, as shown in Figs. 1(a and b), the three normal stresses (σ_z, σ_r, σ_θ) and shear stress ($\sigma_{z\theta}$) components of the stress tensor were modulated. Independent control of the normal and shear stresses allows precise control of the magnitude and direction of the principal stresses on a continuum element. Details of the HCT apparatus used in these experiments are presented elsewhere (Kandasami 2017). Hight et al. (1983) have provided a detailed description on the measurements of average

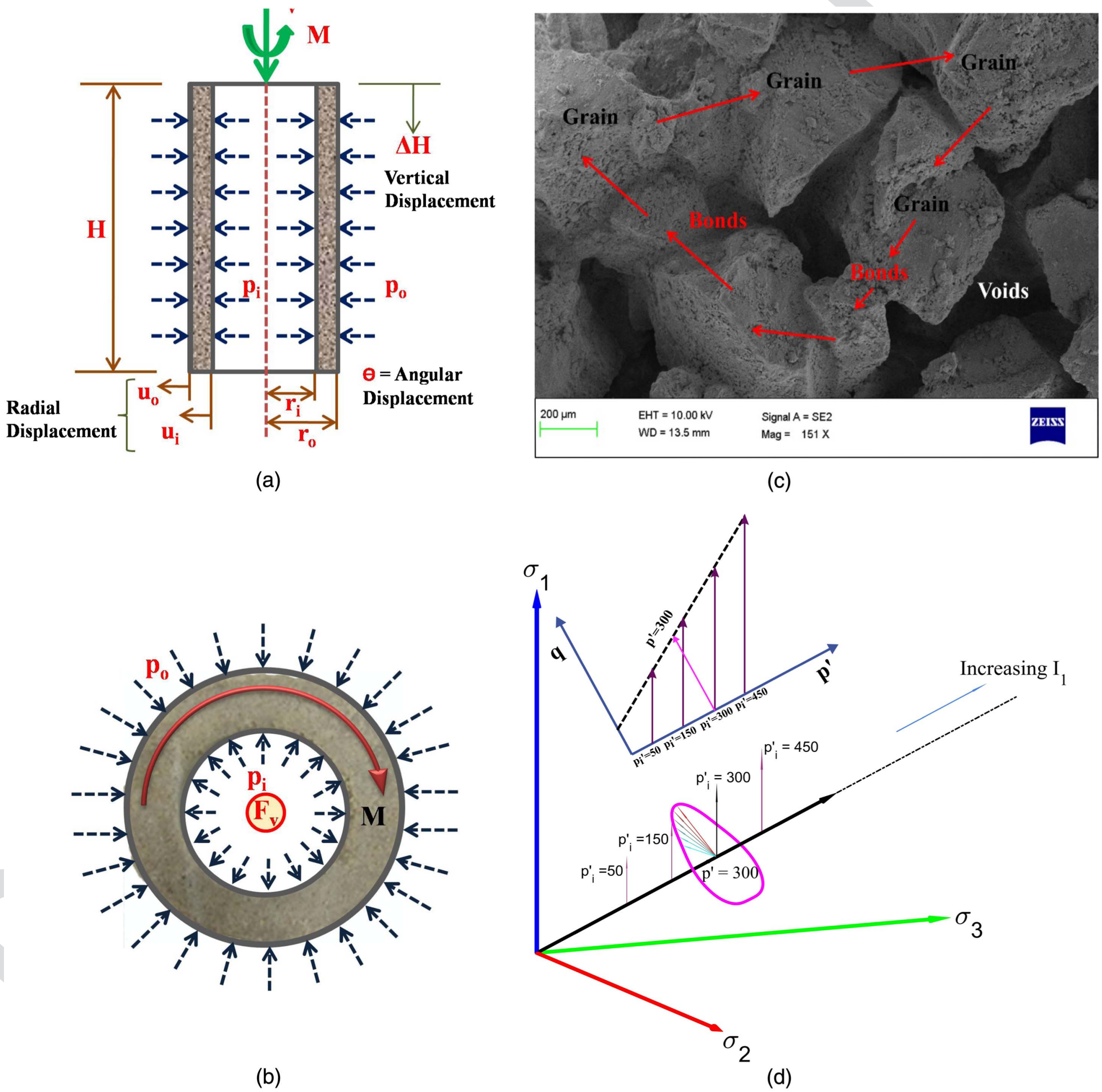

Fig. 1. (a) Sectional view of the hollow cylinder specimen, which is subjected to boundary load, torque, displacements and pressure; (b) top view of the specimen subjected to load and pressures; (c) SEM image of the cemented sand cured for 14 days showing a contact bound structure; and (d) stress path of the conventional triaxial compression tests p_i' and constant p' tests performed at different b.

normal stresses, shear stress, and strains from an HCT elemental test. The average stresses and strains on an element were obtained by solving the balance equations (Kandasami 2017).

Care was taken so that these tests are repeatable under identical boundary conditions. Additionally, the variation of p_i and p_o applied on to the hollow cylinder was kept at minimum so as to reduce the nonuniformities across the specimen. Nakata et al. (1998) had suggested the pressure ratios in the range of $0.75 < p_i/p_o < 1.3$ for the specimen dimensions used in this program to minimize stress nonuniformities. Errors due to membrane penetration, membrane restraint, and end restraint in the measurement of stresses were found to be negligible (Kandasami 2017). Local strain gauges are not utilized in this experimental program because the specimens were sheared to large strains and the emphasis was to study the response at large strains.

Model Material and Specimen Preparation

An angular quartzitic sand is used in this study; the roundness and sphericity of the particles were 0.17 and 0.42, respectively, with a specific gravity of 2.65, mean grain size of 0.45 mm, (Kandasami and Murthy 2017) minimum and maximum porosity was found to be 35% and 49%, respectively, along with ordinary Portland cement (OPC equaling 53 grade, specific gravity of 3.15) as a binding agent.

A specially designed hollow cylinder mold was used for reconstituting the cemented sand in the laboratory (Kandasami 2017). Clean angular sand and 4% ordinary Portland cement by weight of sand was mixed thoroughly under dry conditions. An optimum quantity of water (18% by weight) was added to this dry mixture and homogenized. This mixture was placed in the hollow cylindrical mold and compacted statically until the required density was achieved. After 24 h, the specimen was extruded from the mold and cured under moist conditions for a period of 14 days. The hollow cylinder specimens were cast to a height of 200 mm, an outer diameter of 100 mm, and thickness of 20 mm. The height and thickness of the specimen were fixed based on the recommendations by Saada and Townsend (1981) and Sayao and Vaid (1991) so that stress nonuniformities across the specimen were minimized. [8] Specimens were prepared at two different densities i.e., 1.5 g/cc and 1.6 g/cc (maximum dry density). Fig. 1(c) shows the scanning electron micrograph of the weakly cemented sand used in this study. This material has a contact bound structure (Sowers and Sowers 1951), i.e., sand grains were bonded together through cementation creating an inherent structure.

Testing

An effective stress of 20 kPa was maintained during the saturation process of the specimens. Protocols for reconstitution of the cemented sand and their saturation were followed in this testing program as per the recommendations of Reddy and Saxena (1993) and Black and Lee (1973), respectively. A high back pressure saturation technique was utilized to achieve complete saturation of these cemented specimens. Following saturation, the specimens were isotropically consolidated to a required mean effective stress prior to being sheared under drained conditions. Two broad suites of tests, i.e., conventional triaxial tests, through which the effect of isotropic compression, shear response affected by initial mean effective stress (p_i'), and density was quantified, while a set of constant p' tests were also performed under different stress paths so as to map the yield surface.

Conventional Triaxial Compression Test (p_i')

In this suite of tests, the specimens were initially consolidated to a mean effective stress (p_i') of 50, 150, 300, and 450 kPa and sheared keeping $\sigma_2' = \sigma_3'$ constant while increasing σ_1'. All the specimens were sheared at a displacement rate of 0.1 mm/min (ASTM D5102-09), until the specimen reached a final state. Fig. 1(d) shows [9] the evolution of stresses of a conventional triaxial compression test in the principal stress space corresponding to different p_i'.

Constant p' Test

A series of tests at constant mean effective stress was also performed. The specimens were sheared at different intermediate principal stress ratio (b) (conventionally portrayed using the Lode angle) in order to traverse a specific locus on the octahedral plane. In this set of tests, all the specimens were isotropically consolidated to a mean effective stress of 300 kPa and sheared at this p' keeping the principal stress inclination (α equalling direction of major principal stress with respect to the vertical axis of the specimen) at 0°. Displacement-controlled tests (at 0.10 mm/min) were performed at different b varying from 0 to 1 at 0.2 intervals. The relation between the parameter b and the Lode angle θ (for $\sigma_1' \geq \sigma_2' \geq \sigma_3'$) is given in the Eq. (1) [10]

$$\cos\theta = \frac{2-b}{2\sqrt{b^2-b+1}} \tag{1}$$

Results

A suite of hollow cylinder tests on these weakly cemented sand specimens were performed in order to investigate the effect of density, initial p_i', and intermediate principal stress ratio on the ensemble mechanical behavior. The results are analyzed in plasticity theory framework. Specific focus on the peak stress state and the state of plastic flow (henceforth referred to as "the final state") was given in this study. A summary of the laboratory tests performed in this testing program is provided in Table 1. At low confining pressures, a typical stress strain response observed in case of rocks shows a catastrophic failure once a peak stress is reached (Nygaard et al. 2006), while a weakly cemented sand specimen shows a gradual postpeak softening. The condition where the plastic dilatancy [$D_p = (d\varepsilon_v^p/d\varepsilon_q^p)$ (Kandasami and Murthy 2015)] reaches a negligible value at large deformation was considered necessary condition for final state.

Fig. 2 shows a typical stress strain response of a cemented sand under triaxial compression conditions [octahedral shear stress (τ_{oct}) and volumetric strain (ε_v) with octahedral shear strain (γ_{oct})]. It was observed that octahedral shear stress increases rapidly with octahedral shear strain and reaches the peak value at about 3% shear strain, after which there is a decrease in shear strength and eventually reaches a final state at large strain. When the volumetric strain is observed, they show an initial contraction, following which, a peak value of volumetric strain (contractive) is reached, and the specimen then dilates continuously to reach the final state. It should be noted that the inflection point of the volumetric response (which corresponds to the peak dilatant state) does not coincide with the peak in the octahedral shear stress as would occur in a typical granular material. A detailed discussion about this noncoincidence of peaks and micromechanical interpretation is provided in the ensuing.

Conventional Triaxial Testing

The effect of hydrostatic compression, p_i', and ensemble density on the mechanical response of weakly cemented sand was examined.

Table 1. Test results of the weakly cemented sand at initial densities of 1.6 and 1.5 g/cc for both peak stress state and final stress state

γ_d (g/cc)	P'_i (kPa)	b at $\alpha = 0°$	σ'_1 (kPa)	σ'_2 (kPa)	σ'_3 (kPa)	p' (kPa)	q (kPa)	$H = q/p'$
				At peak stress state: TX-C				
1.6	50	0	458.59	60.51	58.82	192.64	399.76	2.07
1.6	150	0	850.75	160.57	158.89	390.07	691.86	1.77
1.6	300	0	1,456.76	310.87	309.14	692.26	1,147.61	1.65
1.6	450	0	1,838.52	463.46	461.72	921.24	1,376.79	1.49
1.5	50	0	416.71	62.31	62.30	180.44	354.40	1.96
1.5	300	0	1,293.29	347.51	347.51	662.77	945.77	1.42
1.5	450	0	1,606.31	461.02	459.24	842.19	1,147.06	1.36
				At peak stress state: constant p'				
1.6	300	0	707.41	137.97	100.55	315.31	606.86	1.92
1.6	300	0.2	687.60	190.33	66.17	314.70	621.42	1.97
1.6	300	0.4	610.39	284.02	60.93	318.45	549.45	1.72
1.6	300	0.6	559.84	374.62	47.18	327.21	512.66	1.56
1.6	300	0.8	502.48	424.48	61.66	329.54	440.82	1.33
1.6[a]	300	1	497.70	489.18	33.45	340.11	464.25	1.36
1.5	300	0	714.51	106.00	106.00	308.84	608.50	1.97
1.5	300	0.2	679.74	225.70	113.73	339.72	566.00	1.66
1.5	300	0.4	629.99	305.22	94.45	343.22	535.54	1.56
1.5	300	0.6	542.19	358.36	79.37	326.64	462.82	1.41
1.5	300	0.8	511.96	421.21	79.92	337.70	432.03	1.27
1.5[a]	300	1	392.31	473.66	129.88	331.95	262.42	0.79
				At final stress state: TX-C				
1.6	50	0	249.20	58.43	56.72	121.45	192.47	1.58
1.6	150	0	634.71	159.42	159.42	317.85	475.28	1.49
1.6	300	0	1,145.97	300.74	297.04	581.25	848.93	1.46
1.6	450	0	1,515.42	426.07	424.18	788.56	1,091.24	1.38
1.5	50	0	247.19	59.48	57.83	121.50	189.36	1.55
1.5	300	0	983.51	320.80	320.78	541.70	662.72	1.22
1.5	450	0	1,389.41	470.44	470.39	776.73	919.07	1.18
				At final stress state: constant p'				
1.6	300	0	572.93	176.73	175.07	308.24	397.86	1.29
1.6	300	0.2	587.60	219.90	128.20	311.90	459.39	1.47
1.6	300	0.4	559.30	285.15	98.98	314.48	460.32	1.46
1.6	300	0.6	541.04	374.41	82.21	332.55	458.82	1.38
1.6	300	0.8	492.73	391.21	66.25	316.73	426.47	1.34
1.6[a]	300	1	507.68	487.31	53.71	349.57	453.97	1.29
1.5	300	0	616.36	152.57	150.59	306.50	465.76	1.52
1.5	300	0.2	573.96	232.18	148.92	318.35	425.03	1.33
1.5	300	0.4	527.20	265.73	89.97	294.30	437.22	1.48
1.5	300	0.6	500.45	341.30	103.91	315.22	396.54	1.25
1.5	300	0.8	463.84	388.80	72.47	308.37	391.36	1.26
1.5[a]	300	1	401.17	472.97	148.75	340.96	252.42	0.74

Note: γ_d = dry density; P'_i = confining pressure at the start of shearing; b = intermediate principal stress ratio; σ'_1 = major principal stress; σ'_2 = intermediate principal stress; σ'_3 = minor principal stress; p' = mean effective stress; q = deviatoric stress; and H = stress ratio.
[a]Specimens that did not reach a clear final state (failure due to instability).

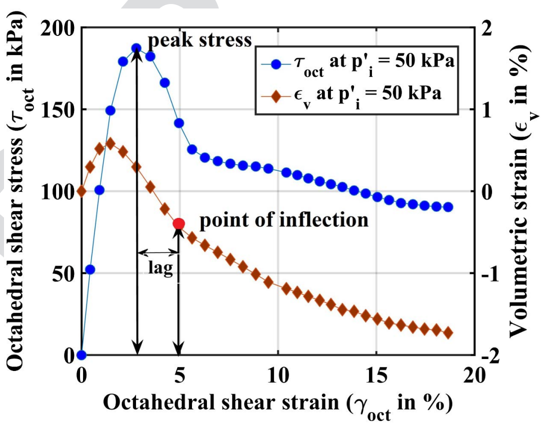

Fig. 2. Typical octahedral shear stress and volumetric strain plot for a conventional triaxial compression test (p'_i of 50 kPa, 1.6 g/cc).

Hydrostatic Compression

A hydrostatic compression test was carried out to quantify the volume change associated with changes in mean effective stress only. Weakly cemented sand specimen ($\gamma = 1.6$ g/cc) was hydrostatically compressed to a mean effective stress of 1 MPa. With an increase in p', the void ratio decreased from 0.68 to 0.64 due to the plastic volumetric contraction of the specimen suggesting that there is a progressive degradation of bonds without shearing (under high hydrostatic compression only). The rate of change of void ratio also decreases with increase in mean effective stress.

Effect of p'_i

The results of the conventional triaxial compression tests are shown in Fig. 3. Fig. 3(a) shows the variation of octahedral shear stress with octahedral shear strain for four tests conducted at p'_i of 50, 150, 300, and 450 kPa. The peak stress increases with increase in $p'_i(I_{1i}/3)$ and the stiffness of these specimens also markedly

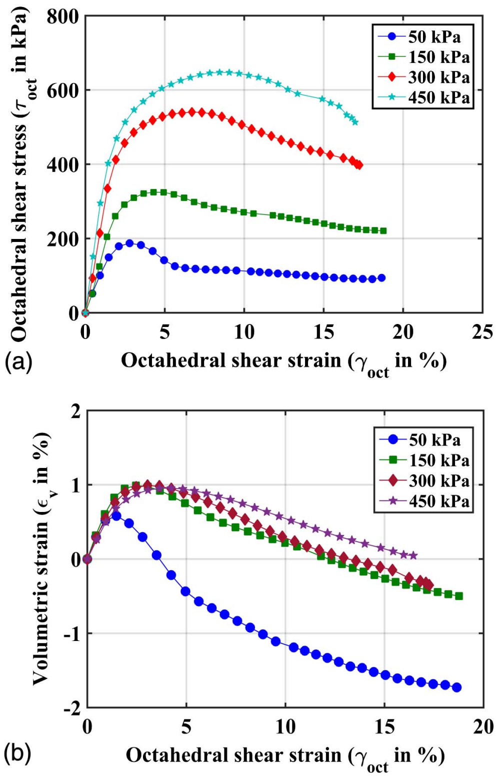

Fig. 3. (a) Variation of octahedral shear stress with octahedral shear strain for triaxial compression tests performed at different p_i' (density of 1.6 g/cc); and (b) volume change response of the cemented sand specimens with octahedral shear strain at different p_i'.

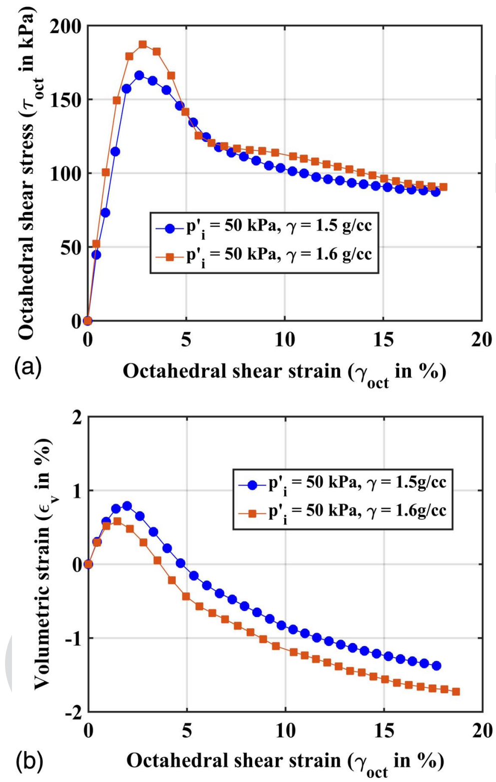

Fig. 4. (a) Effect of density on the peak strength and final state strength at a p_i' of 50 kPa; and (b) volume change response.

increases with p_i' (as also reported by Ismail et al. 2002; Lade and Overton 1989; Leroueil and Vaughan 1990; Marri et al. 2012 on different geomaterials). In these experiments, a three-fold increase in the peak strength was observed as the confining pressure changed from 50 to 450 kPa. When the p_i' was lower than bond strength (114 kPa, intercept from p versus q plot), a clear peak stress was observed followed by a distinct post peak strain softening leading to final state. With an increase in p_i', a distinct peak was not observed, and the response is akin to a loose granular material, and in effect the ductility of the specimen increases with increase in p_i'. Fig. 3(b) shows the corresponding volumetric strain plots for these four tests; all the specimens initially show contraction following which the specimen dilates to reach the final state. Increased p_i' suppresses the dilatancy of the specimen. The strain required to mobilize the peak strength as well as the final state strength increases with increase in p_i'. The octahedral shear strain corresponding to the maximum value of volumetric contraction also increases with increase in p_i'.

Specimens were reconstituted to two different densities, i.e., 1.5 and 1.6 g/cc, and consolidated to different p_i' were also examined. Fig. 4(a) presents the results of two specimens consolidated to the same p_i' (50 kPa) at 1.5 and 1.6 g/cc. The peak strength and the stiffness of the denser specimen is higher. The corresponding volumetric strain is shown in Fig. 4(b). The specimens with lower density show enhanced contractivity compared to denser specimens.

Constant p' Test

Tests were performed at different b values starting from $b = 0$ to 1 at an interval of 0.2 for two different densities, i.e., 1.5 and 1.6 g/cc for mapping the yield locus in principal stress space. Fig. 5(a) shows the variation of octahedral shear stress with octahedral shear strain for weakly cemented sand specimen prepared at a density of 1.6 g/cc. It was observed that the peak stress decreases with increase in b. Even though the peak stress decreases, the stiffness (initial tangent stiffness and not elastic stiffness) of these specimens when tested at different b remained the same. In the small strain regime, this weakly cemented sand stiffness response was found to be isotropic unlike purely frictional granular materials. A similar response was found from the specimens reconstituted at 1.5 g/cc. The peak and final state points obtained from different b tests were used to map the failure locus on the octahedral plane and are discussed in the ensuing. The volumetric response at different b values is plotted in Fig. 5(b). All the specimens initially contracted, reached a peak value, and then dilated to reach the final state.

Discussion

In order to arrive at the state boundary surfaces for these materials, the effect of density, initial confining pressure, and mapping the failure surface by modulating the principal stresses was carried out. Further, the mechanical behavior under two specific states are explored:

1. Peak stress state and the evolving stress dilatancy; and
2. State of plastic flow or the final state.

Peak Stress State and the Evolving Stress-Dilatancy

During shearing, the cemented sand behavior beyond elastic regime, a maximum shear stress in τ_{oct} versus γ_{oct} plot, was identified, during which the breakdown of weak cohesive bonds between

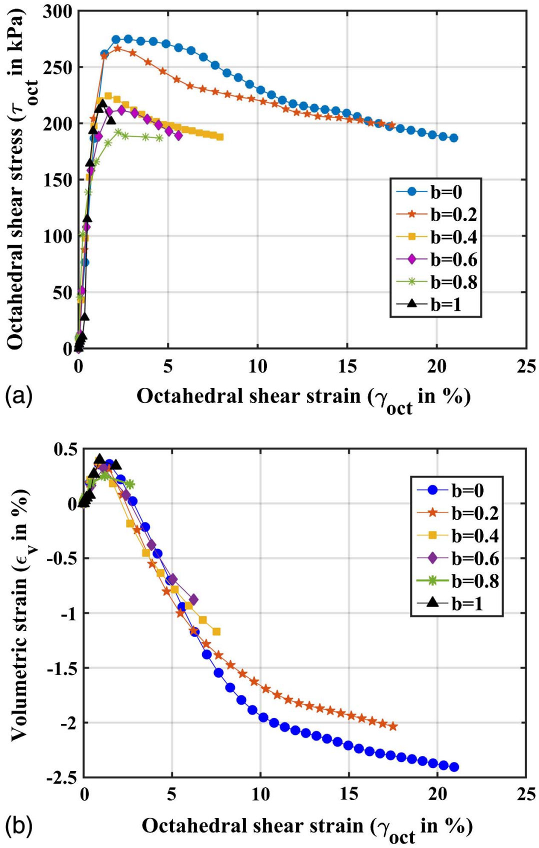

Fig. 5. (a) Effect of b on the mechanical response of weakly cemented sand (constant p' and $\alpha = 0°$); and (b) volumetric strain response of weakly cemented sand at different b.

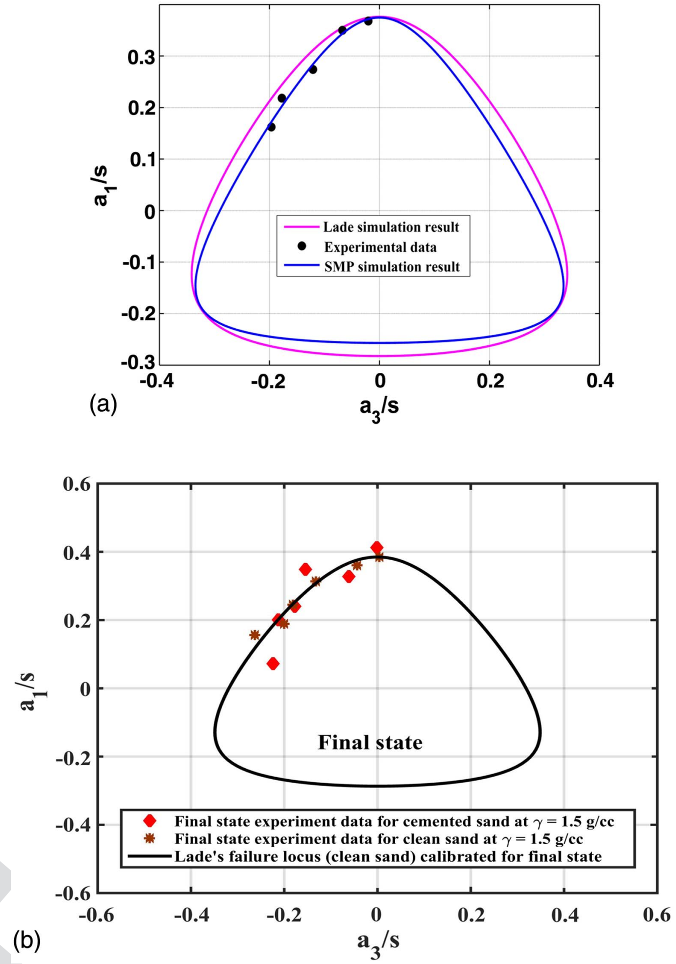

Fig. 6. (a) Peak stress state obtained by variation of b for cemented sand at a density of 1.6 g/cc and constant $p' = 300$ kPa presented on deviatoric plane along with Lade's and SMP failure criterion; and (b) final state obtained from the tests performed on cemented sand (1.5 g/cc) is plotted along with the final state of clean sand at same density from Kandasami and Murthy (2015).

the particulates increases rapidly. This breakdown of cementation between the grains leads to the formation of clumps of decemented clusters, which eventually results in increased volume (Wang and Leung 2008a, b; Bono et al. 2014). Alternatively, this can be construed as the energy required to shear a cemented granular ensemble is distributed between bond breakage and subsequent dilation post peak. Through the DEM simulations, Wang and Leung (2008a) suggest that the breakdown of cementation is initiated before the peak stress state and extends well beyond the peak state. With continued breakdown of cementation, the formation of individual particulates contributes to the strength in addition to an increased volume of the ensemble.

At small strains, breakage of the cementation occurs at few discrete locations; with an increase in the strains, these decemented clusters coalesce to form a localized shear zone beyond the peak stress (Wang and Leung 2008a). At an ensemble level, this peak stress state is considered as a failure. In case of purely frictional materials, the failure locus starts from the origin of principal stress space whereas for weakly cemented materials, which possess a bond strength of σ_t, the locus originates from $(-\sigma_t, -\sigma_t, -\sigma_t)$ (Gao and Zhao 2012; Lade and Kim 1988; Kim and Lade 1984; Yao et al. 2004).

The 3D stress state is represented in two dimensions [Fig. 6(a)] by rotating the intermediate principal stress so as to coincide with the hydrostatic axis, which places the other two axes on the deviatoric plane (Atkinson and Bransby 1977; Schofield and Wroth 1968). The variables used in this representation of the two-dimensional (2D) plane are presented in Eqs. (2)–(4)

$$a_1 = \frac{2\sigma_1' - \sigma_2' - \sigma_3'}{\sqrt{6}} \quad (2)$$

$$a_3 = \frac{\sigma_3' - \sigma_2'}{\sqrt{2}} \quad (3)$$

$$S = \sigma_1' + \sigma_2' + \sigma_3' \quad (4)$$

In this study, two failure criteria, Lade's failure criterion (Kim and Lade 1988) and the SMP failure criterion (Matsuoka and Nakai 1974) as given in Eq. (5), were considered and benchmarked for its validity using the experimentally determined peak stress states. It should be noted that both these yield criteria are coincident when $a_3/S = 0$

$$\left(\frac{I_1^3}{I_3} - 27\right)\left(\frac{I_1}{P_a}\right)^m = \widehat{\eta} \quad \text{(Lade failure criterion)}$$
$$\frac{I_1 I_2}{I_3} = \widehat{c} \quad \text{(SMP failure criterion)} \quad (5)$$

where $\widehat{\eta} = 27.92$; $m = 0.105$- for Lade; and $\widehat{c} = 15.8$ for SMP were obtained from the experiments. Fig. 6(a) shows the deviatoric plane at a mean effective stress of 300 kPa where the SMP failure criterion provides a slightly better match with the experimental results and is circumscribed by the Lade failure criterion.

For understanding the response of cemented sand beyond the peak stress state, a plot of the stress ratio (η) versus dilatancy (D_p) (Been and Jefferies 2004) is examined. These plots show the evolution of stresses and state of cemented sand during the shearing process as presented in Figs. 7(a and b). The peak stress ratio and maximum dilatancy decreases with increase in p_i'. Cecconi and Viggiani (2001) reason that there is progressive suppression of microcracking with increasing p_i' due to which the specimens exhibit a predominantly ductile behavior. An interesting manifestation of cementation breakage and subsequent dilation is that the peak stress ratio [A in Fig. 7(a)] and peak dilatant state [B in Fig. 7(a)] do not coincide, contrary to a typical frictional granular ensemble. This noncoincidence lag (Fig. 2) was quantified as a difference between the shear strain corresponding to peak stress state and maximum dilatancy state (point of inflection). This lag increases with increase in p_i' as shown in Fig. 7(d). The difference in volumetric dilation between A and B [$D_p(A) - D_p(B)$] decreases with increase in p_i' [Fig. 7(a)].

The intermediate principal stress ratio has no effect on the elastic response of cemented sand, because the cementation between the grains offers a structure to the ensemble. Beyond the peak state, b has a significant influence on the overall mechanical behavior [Fig. 7(c)]. The peak stress ratio decreases with increase in b. The lag also decreases with an increase in b as shown in Fig. 7(d). In interpreting the results, the stress state at $b = 0$ is referred to as a compressive state, while $b = 1$ represents a tensile state. As the stress path moves from compressive to a tensile state, the brittleness increases (Fig. 5). During compression, simultaneously operative mechanisms of bond breakage and particle rearrangement contribute to the strength of the cemented sand. In case of tensile stress state, only the cohesive bonds between the particles contribute to the strength, due to which an increased brittleness is observed (Nova and Zaninetti 1990).

Final Stress State

With continued shearing, at large strains the stress state at which D_p tends towards zero/negligible value is referred to as the final stress state. This state is indicative of a purely frictional response due to intergrain interaction with negligible bond breakage or dilation.

The final state identified from all the drained triaxial compression tests is plotted in the Fig. 8. Specimens initially reconstituted to different densities, once sheared to the final state emerged as destructured sand with different gradations. The initial reconstitution density controls the amount of destructuring occurred in the specimen when sheared to large strains. This destructured cemented sand when examined in the $e - p'$ space shows different final state loci depending on the initial reconstitution density. These nonunique final state loci [in e versus $(p_i'/p_a)^{\alpha}$] are very similar to observations made on the mechanics of sand with fines (Murthy et al. 2007). When visualized in the stress space, the final state friction angle changes with initial reconstitution density, which is consistent with the observation from, Fig. 8. The representation of the steady state locus given by Li and Wang (1998) was used for

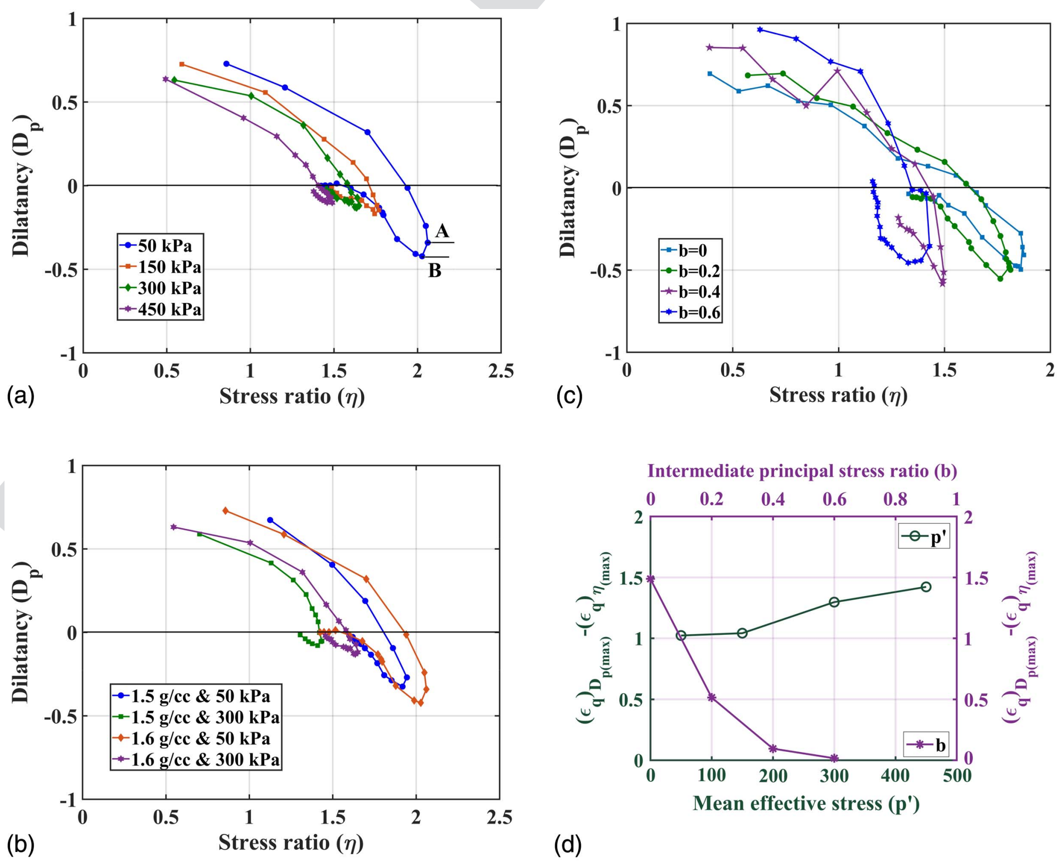

Fig. 7. Stress-dilatancy response for (a) different p_i' at a density of 1.6 g/cc; (b) different densities (1.5 and 1.6 g/cc) at two mean effective stresses (50 and 300 kPa); (c) different b values varying from 0 to 0.6 at 0.2 intervals (1.6 g/cc and $p_i' = 300$ kPa); and (d) the shear strain difference between peak stress ratio and maximum value of dilation (lag) with different b and p'.

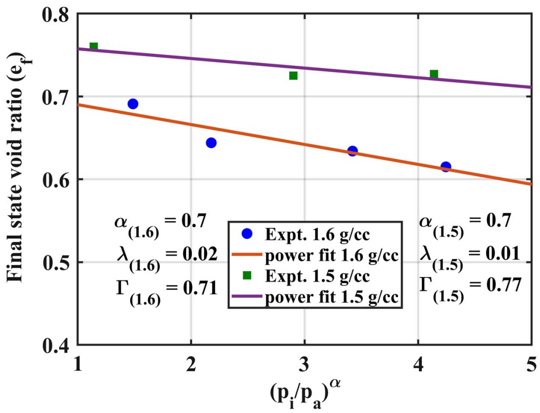

Fig. 8. Final state locus in e versus p_i'/p_a for weakly cemented sand with 4% cementation.

these experimental data. The locus in the $e - \log p'$ state space is a power function as shown in Eq. (6)

$$e_{CS} = \Gamma - \lambda \left(\frac{p'}{P_a}\right)^{\alpha} \tag{6}$$

where P_a = reference stress (atmospheric pressure); and Γ, λ, and α = fitting parameters.

A similar exercise of representing the locus of final state stresses in deviatoric plane is presented in Fig. 6(b). A comparison plot of the final state experimental points obtained at different b for clean sand (Kandasami and Murthy 2015) and weakly cemented sand at the same density is shown in Fig. 6(b). This comparison is possible because the behavior of the weakly cemented sand at 300 kPa is ductile in nature (except at $b = 1$) without the formation of clear shear bands or localization. The Fig. 6(b) also shows Lade's failure locus for clean sand. The behavior of the destructured weakly cemented sand at final state is akin to that of clean sand. Because the sample is sheared towards the final state, cohesive bonds progressively break down to form decemented clusters. These decemented clusters are interacting through purely frictional interactions (Wang and Leung 2008a).

Model Description

In modeling cemented sand, cementation has been hypothesized as an additional confinement on sand (Kim and Lade 1988; Gens and Nova 1993; Abdulla and Kiousis 1997b; Vatsala et al. 2001; Gao and Zhao 2012). Among these models, Lade's model (which has been widely applied over a range of materials including sand, cemented sand, concrete, etc.) is used in this study. This exercise is undertaken to understand if this Lade's model is viable for prediction of the response of weakly cemented sand.

A brief description of Lade's model is provided, after which a few prediction exercises are performed in order to check the efficacy of this model with the experimental results. This model (Kim and Lade 1988; Lade 1977; Lade and Duncan 1975) was originally proposed for frictional materials, subsequently extended for c-φ material by translating the stress space along the hydrostatic axis to account for the tensile strength due to the cementation between the grains. The stress state is transformed to $\underline{\sigma} = \underline{\sigma}' + \sigma_t \underline{I}$, where $\underline{\sigma}'$ is the original stress tensor for a c-φ material with tensile strength (i.e., $\sigma_t = aP_a$, where a is failure parameter and P_a is the atmospheric pressure). The invariants of transformed stress tensor ($\underline{\sigma}$) are I_1, I_2, I_3.

Elastic Stress-Strain Relation

$$d\underline{\sigma} = C^e d\underline{\varepsilon} \tag{7}$$

where $C^e = \lambda' \underline{I} \otimes \underline{I} + 2\mu' \mathbb{S}$, λ' and μ' are Lame's constants given by $\lambda' = (Ev/(1+v)(1-2v))$ and $\mu' = (E/2(1+v))$; $\underline{I}$ = second order identity tensor; $\mathbb{S}$ = fourth order symmetrizer tensor; and ν = Poisson's ratio. The elastic modulus E is given as

$$E(\underline{\sigma}) = MP_a \left[\left(\frac{I_1}{P_a}\right)^2 + 6\frac{(1+\nu)}{(1-2\nu)}\frac{J_2}{P_a}\right]^{\lambda'} \tag{8}$$

where $J_2 = (1/2)tr\,\underline{s}^2$ = second invariant of the deviatoric transformed stress tensor $\underline{s} = (\underline{\sigma} - (I_1/3)\underline{I})$; and M, λ', and ν = elastic model parameters.

Failure Criterion

Failure is defined as the peak of $q - \varepsilon_a$, where $q = \sqrt{3J_2}$ and ε_a is the axial strain. Failure function $F(\underline{\sigma})$ is given [Eq. (9)] as

$$F(\underline{\sigma}) = f_n(\underline{\sigma}) - \widehat{\eta}, \qquad f_n(\underline{\sigma}) = \left(\frac{I_1^3}{I_3} - 27\right)\left(\frac{I_1}{P_a}\right)^m \tag{9}$$

At failure, $F(\underline{\sigma}) = 0$. m and $\widehat{\eta}$ are the failure parameters. The failure criterion delineates the hardening regime from softening regime through stress level $S \in (0,1)$ defined as $S = (f_n/\eta)$.

Flow Rule

A nonassociated flow rule $(d\underline{\varepsilon}^p = d\lambda(\partial g_p(\underline{\sigma})/\partial \underline{\sigma})$ is employed to calculate the incremental plastic strains. The form of plastic potential function $(g_p(\underline{\sigma}))$ is given in Eq. (10)

$$g_p(\underline{\sigma}) = \left(\psi_1 \frac{I_1^3}{I_3} - \frac{I_1^2}{I_2} + \psi_2\right)\left(\frac{I_1}{P_a}\right)^{\mu} \tag{10}$$

where ψ_1, ψ_2, and μ are the plastic potential parameters.

Yield Criterion and Work Hardening/Softening Function

The function $f(\underline{\sigma}, W_p)$ is the yield function given by

$$f(\underline{\sigma}, W_p) = f_1(\underline{\sigma}) - f_2(W_p) \tag{11}$$

with yield function $f_1(\underline{\sigma})$ defined as

$$f_1(\underline{\sigma}) = \left(\psi_1 \frac{I_1^3}{I_3} - \frac{I_1^2}{I_2}\right)\left(\frac{I_1}{P_a}\right)^h \exp(q) \tag{12}$$

$$q = \frac{\alpha S}{1 - (1-\alpha)S} \quad q \in (0,1) \tag{13}$$

where h and α = yield parameters.

The function $f_2(W_p)$ is defined as follows.

For the hardening regime:

$$f_2(W_p) = \left(\frac{W_p}{DP_a}\right)^{\frac{1}{\rho}} \tag{14}$$

where W_p = plastic work done, defined as $W_p = \int \underline{\sigma}{:}d\underline{\varepsilon}^p$

$$D = \frac{C}{(27\psi_1 + 3)^{\rho}} \qquad \rho = \frac{p}{h} \tag{15}$$

where C and p are defined for plastic work in isotropic compression test as

$$W_p^{iso} = CP_a \left(\frac{I_1}{P_a} \right)^p \tag{16}$$

For the softening regime:

$$f_2(W_p) = A \exp\left(-B \frac{W_p}{P_a} \right) \tag{17}$$

where C, p, A, B = hardening/softening parameters.

Lade's Model Predictions and Comparisons

Lade's constitutive model requires 13 material parameters to capture the material response. These 13 parameters were obtained using laboratory triaxial compression and isotropic compression experiments on the model frictional or c-φ material (Kim and Lade 1988; Lade and Kim 1988a, b). The procedure for determining these material parameters from the experimental data are provided in Kim and Lade (1988) and Lade and Kim (1988a, b). The material parameters obtained for the weakly cemented sand, used in this study, for the density 1.6 g/cc are as follows. The elastic parameters ($\nu = 0.23$, $M = 456.89$, $\lambda = 0.265$), failure parameters ($a = 1.125$, $m = 0.105$, $\widehat{\eta} = 27.92$), plastic potential parameters ($\psi_1 = 0.027$, $\psi_2 = -3.62$, $\mu = 2.552$), hardening parameters ($C = 0.00035$, $p = 1.6$), and yield parameters ($h = 1.056$, $\alpha = 0.065$). The experimental results are compared with model predictions for different p_i', density, and b.

Fig. 9 shows a comparison of model prediction and experimental results of octahedral shear stress and volumetric strain with octahedral shear strain at two different p_i' (300 and 450 kPa). At small strain, the strength and volumetric response are well in accord with experimental results. With further increase in strain, the predicted strength slightly deviates postpeak [Fig. 9(a)], while volumetric response at larger strains is not captured well because the model

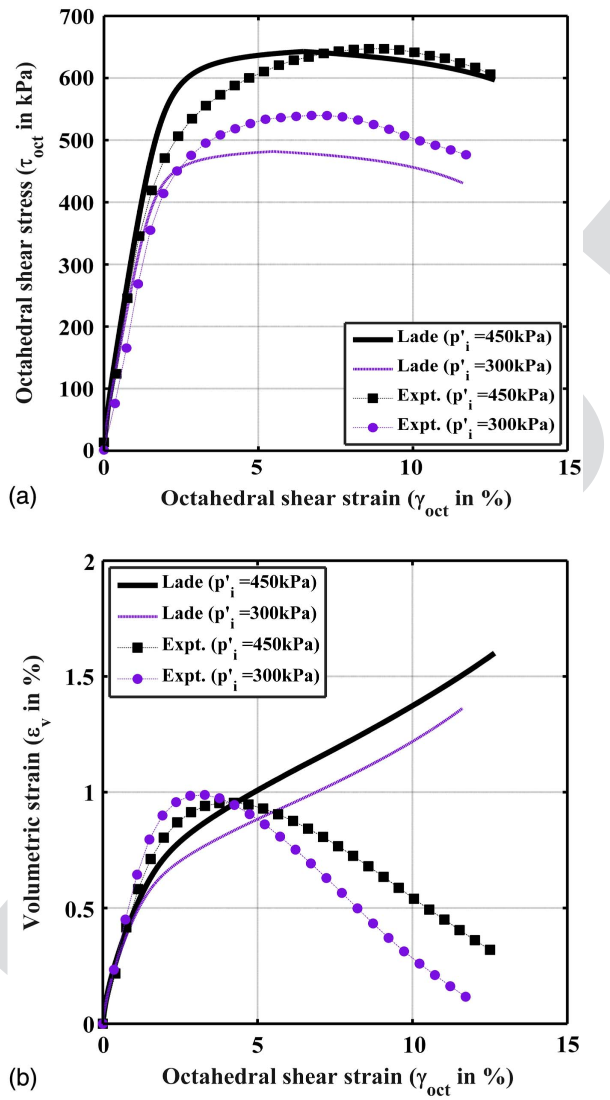

Fig. 9. Effect of p_i' at a density of 1.6 g/cc—experimental results compared with predictions using Lade's failure criterion: (a) variation of octahedral shear stress with strain; and (b) volumetric strain response of this weakly cemented sand.

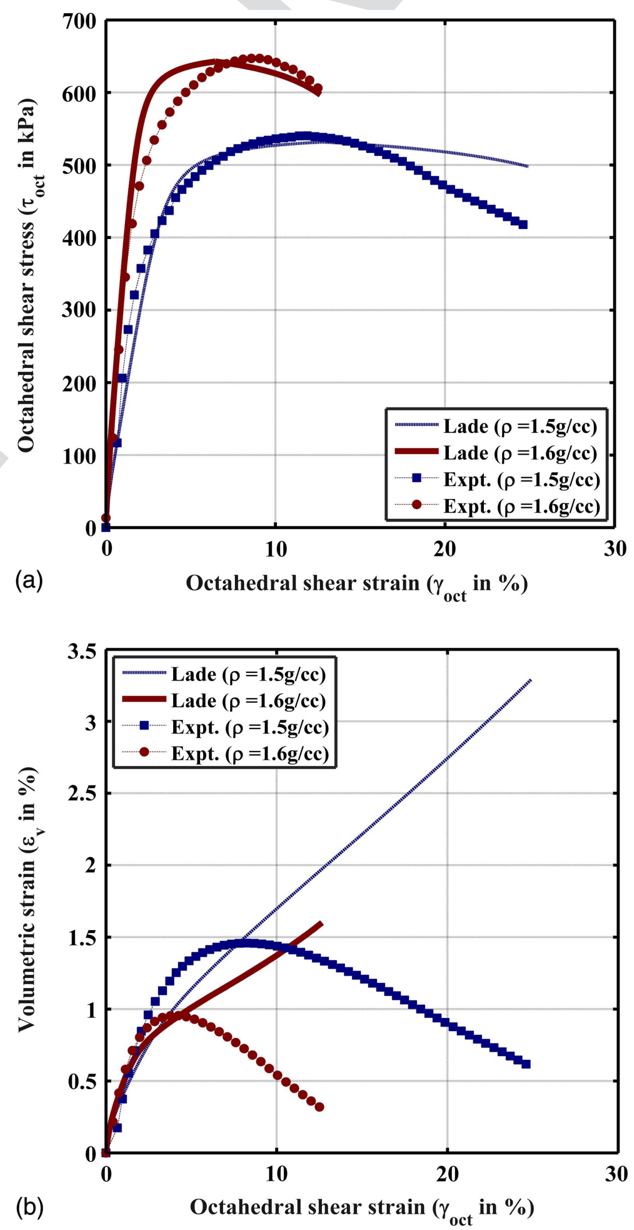

Fig. 10. Effect of density at p_i' of 450 kPa—experimental results compared with prediction using Lade's failure criterion: (a) variation of octahedral shear stress with octahedral shear strain; and (b) volumetric strain behavior of weakly cemented sand.

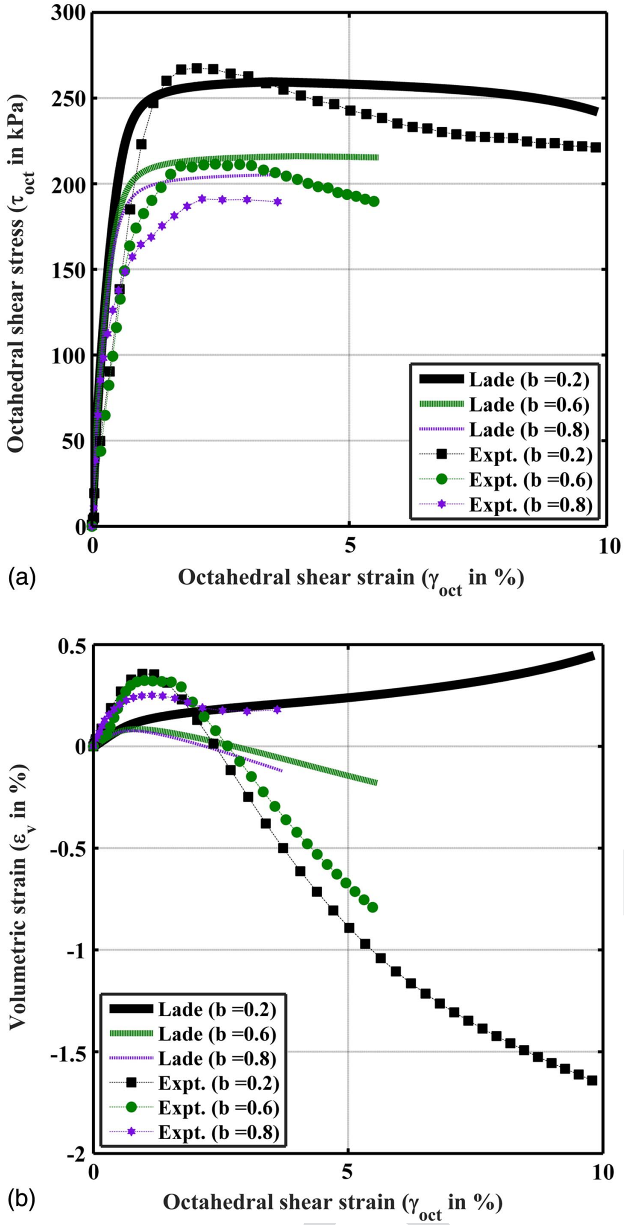

Fig. 11. Effect of b at a constant mean effective stress of 300 kPa and a density of 1.6 g/cc—experimental results compared with predictions using Lade's failure criterion: (a) variation of octahedral shear stress with octahedral shear strain; and (b) volumetric strain behavior of weakly cemented sand.

predicts only contraction and no dilation [Fig. 9(b)]. Similar observations can be made for the effect of density on both stress and volumetric response as shown in Figs. 10(a and b), respectively. For the constant p' tests performed at different intermediate principal stress ratio, the predicted strength response is similar to response of an elastic-perfectly plastic material as shown in Fig. 11(a). The model fails to predict volumetric behavior at higher strain levels [Fig. 11(b)].

This model considers the effect of cementation as a linear translation of the yield surface along the hydrostatic axes. This translation can be recognized as an "artificial increase in the confining pressure over a hypothetical frictional ensemble." With such simplistic treatment of cohesion, the strength of weakly cemented sand and the corresponding volumetric strains at small strain ranges can be adequately predicted (Reddy and Saxena 1992; Lade and Kim 1988a; Abdulla and Kiousis 1997b). At large strains, even though the strength can be adequately predicted, the corresponding volumetric response is not well captured. The artificial increase in confining pressure leads to increased contraction, as is true for a typical frictional material, while in reality, the cemented sand undergoes destructuring, debonding, and consequent dilation. Thus, the predicted response is deviant from the experimental behavior especially at large strains.

Concluding Remarks

The results of this experimental program using the hollow cylinder tests for understanding the mechanical behavior of weakly cemented sand are presented. The addition of small amounts of cementation to a granular ensemble drastically changes the mechanical behavior, in addition to being affected by the density, initial mean effective stress, and intermediate principal stress ratio.

When cemented sand is sheared, following an initial elastic response, a peak stress state is usually observed, which signals the major breakdown of cementation. With continued shearing, further breakdown of the cementation occurs, leading to decemented sand at the final state.

The initial elastic stiffness of these weakly cemented sand increases with increase in initial mean effective stress and density; however, the initial stiffness remains unaffected by b, indicating an initial isotropic fabric due to the cementation.

Observations of the peak stress and the postpeak softening from the series of tests shows ductile or brittle characteristics, depending on the density, initial mean effective stress, and b. The tests conducted at various b values allowed a mapping of the failure surface in the principal stress space, which fits the failure criterion of Lade and SMP models.

The behavior was further characterized by studying the evolving stress dilatancy characteristics of the weakly cemented sand. Lag in the occurrence of the peak in stress ratio and the maximum value of dilation which is a consequence of the inter-granular cementation breakdown is affected by b and initial mean effective stress. The final state loci is nonunique due to the differential destructuring dependent on the initial reconstitution density.

Further, a series of predictions of the mechanical behavior of cemented geomaterials using an elastic-plastic constitutive model of Kim and Lade (1988) was carried out and compared with the experimental response. The model considers the effect of cementation as an additional confinement to the ensemble. Such an approach predicts the stress state fairly well but does not predict the volumetric response, especially beyond the peak stress state accurately for the weakly cemented sand.

Data Availability Statement

Some or all of the data, models, or code generated or used during the study are available from the corresponding author by request.

References

Abdulla, A. A., and P. D. Kiousis. 1997a. "Behavior of cemented sands—I. Testing." *Int. J. Numer. Anal. Methods Geomech.* 21 (8): 533–547. https://doi.org/10.1002/(SICI)1096-9853(199708)21:8<533::AID-NAG889>3.0.CO;2-0.

Abdulla, A. A., and P. D. Kiousis. 1997b. "Behavior of cemented sands—II. Modelling." *Int. J. Numer. Anal. Methods Geomech.* 21 (8):

549–568. https://doi.org/10.1002/(SICI)1096-9853(199708)21:8<549::AID-NAG890>3.0.CO;2-7.

Airey, D. W. 1993. "Triaxial testing of naturally cemented carbonate soil." *J. Geotech. Eng.* 119 (9): 1379–1398. https://doi.org/10.1061/(ASCE)0733-9410(1993)119:9(1379).

Atkinson, J. H., and P. L. Bransby. 1977. *The mechanics of soils, an introduction to critical state soil mechanics*. New York: McGraw-Hill.

Been, K., and M. Jefferies. 2004. "Stress dilatancy in very loose sand." *Can. Geotech. J.* 41 (5): 972–989. https://doi.org/10.1139/t04-038.

Bishop, A. W. 1966. "The strength of soils as engineering materials." *Géotechnique* 16 (2): 91–130. https://doi.org/10.1680/geot.1966.16.2.91.

Black, D. K., and K. L. Lee. 1973. "Saturating laboratory samples by back pressure." *J. Soil Mech. Found. Div.* 99 (1): 75–93. [14]

Bono, J. P., G. R. McDowell, and D. Wanatowski. 2014. "DEM of triaxial tests on crushable cemented sand." *Granular Matter* 16 (4): 563–572. https://doi.org/10.1007/s10035-014-0502-8.

Burland, J. B. 1990. "On the compressibility and shear strength of natural clays." *Géotechnique* 40 (3): 329–378. https://doi.org/10.1680/geot.1990.40.3.329.

Carraro, J. A. H., and R. Salgado. 2004. *Mechanical behavior of non-textbook soils (literature review)*. Joint Transportation Research Program Project No. C-36-50X. West Lafayette, IN: Purdue Univ.

Cecconi, M., and G. Viggiani. 2001. "Structural features and mechanical behaviour of a pyroclastic weak rock." *Int. J. Numer. Anal. Methods Geomech.* 25 (15): 1525–1557. https://doi.org/10.1002/nag.185.

Clough, G. W., N. S. Rad, R. C. Bachus, and N. Sitar. 1981. "Cemented sands under static loading." *J. Geotech. Eng. Div.* 107 (Jun): 799–817. [15]

Coop, M. R., and J. H. Atkinson. 1993. "The mechanics of cemented carbonate sands." *Géotechnique* 43 (1): 53–67. https://doi.org/10.1680/geot.1993.43.1.53.

Fernandez, A. L., and J. C. Santamarina. 2001. "Effect of cementation on the small-strain parameters of sands." *Can. Geotech. J.* 38 (1): 191–199. https://doi.org/10.1139/t00-081.

Gao, Z. W., and J. D. Zhao. 2012. "Constitutive modeling of artificially cemented sand by considering fabric anisotropy." *Comput. Geotech.* 41 (Apr): 57–69. https://doi.org/10.1016/j.compgeo.2011.10.007.

Gens, A., and R. Nova. 1993. "Conceptual bases for a constitutive model for bonded soils and weak rocks." *Geotech. Eng. Hard Soils-Soft Rocks* 1 (Oct): 485–494. [16]

Hight, D. W., A. Gens, and M. J. Symes. 1983. "The development of a new hollow cylinder apparatus for investigating the effects of principal stress rotation in soils." *Géotechnique* 33 (4): 355–383. https://doi.org/10.1680/geot.1983.33.4.355.

Huang, J. T., and D. W. Airey. 1998. "Properties of artificially cemented carbonate sand." *J. Geotech. Geoenviron. Eng.* 124 (Oct): 492–499. https://doi.org/10.1061/(ASCE)1090-0241(1998)124:6(492).

Ismail, M. A., H. A. Joer, W. H. Sim, and M. F. Randolph. 2002. "Effect of cement type on shear behavior of cemented calcareous soil." *J. Geotech. Geoenviron. Eng.* 128 (6): 520–529. https://doi.org/10.1061/(ASCE)1090-0241(2002)128:6(520).

Kandasami, R. K. 2017. *Experimental studies on the mechanical behaviour of cohesive frictional granular materials*. Bengaluru, India: Indian Institute of Science.

Kandasami, R. K., and T. G. Murthy. 2015. "Experimental studies on the influence of intermediate principal stress and inclination on the mechanical behaviour of angular sands." *Granular Matter* 17 (2): 217–230. https://doi.org/10.1007/s10035-015-0554-4.

Kandasami, R. K., and T. G. Murthy. 2017. "Manifestation of particle morphology on the mechanical behaviour of granular ensembles." *Granular Matter* 19 (2): 21. https://doi.org/10.1007/s10035-017-0703-z.

Kim, M. K., and P. V. Lade. 1984. "Modelling rock strength in three dimensions." *Int. J. Rock Mech. Min. Sci. Geomech.* 21 (1): 21–33. https://doi.org/10.1016/0148-9062(84)90006-8.

Kim, M. K., and P. V. Lade. 1988. "Single hardening constitutive model for frictional materials: I. Plastic potential function." *Comput. Geotech.* 5 (4): 307–324. https://doi.org/10.1016/0266-352X(88)90009-2.

Lade, P. V. 1977. "Elasto-plastic stress-strain theory for cohesionless soil with curved yield surfaces." *Int. J. Solids Struct.* 13 (11): 1019–1035. https://doi.org/10.1016/0020-7683(77)90073-7.

Lade, P. V., and J. M. Duncan. 1975. "Elastoplastic stress-strain theory for cohesionless soil." *J. Geotech. Eng. Div.* 101 (Oct): 1037–1053. [17]

Lade, P. V., and M. K. Kim. 1988a. "Single hardening constitutive model for frictional materials II. Yield critirion and plastic work contours." *Comput. Geotech.* 6 (1): 13–29. https://doi.org/10.1016/0266-352X(88)90053-5.

Lade, P. V., and M. K. Kim. 1988b. "Single hardening constitutive model for frictional materials III. Comparisons with experimental data." *Comput. Geotech.* 6 (1): 31–47. https://doi.org/10.1016/0266-352X(88)90054-7.

Lade, P. V., and D. D. Overton. 1989. "Cementation effects in frictional materials." *J. Geotech. Eng.* 115 (10): 1373–1387. https://doi.org/10.1061/(ASCE)0733-9410(1989)115:10(1373).

Leroueil, S., and P. R. Vaughan. 1990. "The general and congruent effects of structure in natural soils and weak rocks." *Géotechnique* 40 (3): 467–488. https://doi.org/10.1680/geot.1990.40.3.467.

Li, X. S., and Y. Wang. 1998. "Linear representation of steady-state line for sand." *J. Geotech. Geoenviron. Eng.* 124 (2): 1215–1217. https://doi.org/10.1061/(ASCE)1090-0241(1998)124:12(1215).

Marri, A., D. Wanatowski, and H. S. Yu. 2012. "Drained behaviour of cemented sand in high pressure triaxial compression tests." *Geomech. Geoeng.* 7 (3): 159–174. https://doi.org/10.1080/17486025.2012.663938.

Matsuoka, H., and T. Nakai. 1974. "Stress-deformation and strength characteristics of soil under three different principal stresses." In *Proc., Japan Society of Civil Engineers*, 59–70. Tokyo: Japan Society of Civil Engineers.

Murthy, T. G., D. Loukidis, J. A. Carraro, M. Prezzi, and R. Salgado. 2007. "Undrained monotonic response of clean and silty sands." *Géotechnique* 57 (3): 273–288. https://doi.org/10.1680/geot.2007.57.3.273.

Nakata, Y., M. Hyodo, H. Murata, and N. Yasufuku. 1998. "Flow deformation of sands subjected to principal stress rotation." *Soils Found.* 38 (2): 115–128. https://doi.org/10.3208/sandf.38.2_115.

Nova, R., and A. Zaninetti. 1990. "An investigation into the tensile behaviour of a schistose rock." *Int. J. Rock Mech. Min. Sci.* 27 (4): 231–242. https://doi.org/10.1016/0148-9062(90)90526-8.

Nygaard, R., M. Gutierrez, R. K. Bratli, and K. Hoeg. 2006. "Brittle–ductile transition, shear failure and leakage in shales and mudrocks." *Mar. Pet. Geol.* 23 (1): 201–212. https://doi.org/10.1016/j.marpetgeo.2005.10.001.

O'Rourke, T. D., and E. Crespo. 1988. "Geotechnical properties of cemented volcanic soil." *J. Geotech. Eng.* 114 (10): 1126–1147. https://doi.org/10.1061/(ASCE)0733-9410(1988)114:10(1126).

Rad, N. S., and G. W. Clough. 1982. *The influence of cementation on the static and dynamic behavior of sands*. Stanford, CA: John A. Blume Earthquake Engineering Center.

Reddy, K. R., and S. K. Saxena. 1992. "Constitutive modeling of cemented sand." *Mech. Mater.* 14 (2): 155–178. https://doi.org/10.1016/0167-6636(92)90012-3.

Reddy, K. R., and S. K. Saxena. 1993. "Effects of cementation on stress-strain and strength characteristics of sands." *Soils Found.* 33 (4): 121–134. https://doi.org/10.3208/sandf1972.33.4_121.

Saada, A. S., and F. C. Townsend. 1981. "State of the art: Laboratory strength testing of soils." In *Laboratory shear strength of soil*. West Conshohocken: ASTM.

Sayao, A. S. F. J., and Y. P. Vaid. 1991. "A critical assessment of stress nonuniformities in hollow cylinder test specimens." *Soils Found.* 31 (1): 60–72. https://doi.org/10.3208/sandf1972.31.60.

Schnaid, F., P. D. M. Prietto, and N. C. Consoli. 2001. "Characterization of cemented sand in triaxial compression." *J. Geotech. Geoenviron. Eng.* 127 (10): 857–868. https://doi.org/10.1061/(ASCE)1090-0241(2001)127:10(857).

Schofield, A., and P. Wroth. 1968. *Critical state soil mechanics*. London: McGraw-Hill.

Sowers, G. B., and G. F. Sowers. 1951. "Introductory soil mechanics and foundations." *Soil Sci.* 72 (5): 405. https://doi.org/10.1097/00010694-195111000-00014.

Vatsala, A., R. Nova, and B. S. Murthy. 2001. "Elastoplastic model for cemented soils." *J. Geotech. Geoenviron. Eng.* 127 (8): 679–687. https://doi.org/10.1061/(ASCE)1090-0241(2001)127:8(679).

Wang, Y. H., and S. C. Leung. 2008a. "Characterization of cemented sand by experimental and numerical investigations." *J. Geotech. Geoenviron. Eng.* 134 (7): 992–1004. https://doi.org/10.1061/(ASCE)1090-0241(2008)134:7(992).

Wang, Y. H., and S. C. Leung. 2008b. "A particulate-scale investigation of cemented sand behavior." *Can. Geotech. J.* 45 (1): 29–44. https://doi.org/10.1139/T07-070.

Yao, Y., D. Lu, A. Zhou, and B. Zou. 2004. "Generalized non-linear strength theory and transformed stress space." *Sci. China Ser. E: Technol. Sci.* 47 (6): 691–670. https://doi.org/10.1360/04ye0199.

